TENSILE AND WATER ABSORPTION BEHAVIOUR OF POLYBENZOXAZINE / HEMP FIBRES COMPOSITES: EXPERIMENTAL ANALYSIS AND THEORETICAL VALIDATION

A. Q. DAYO[a,b], S. ULLAH[c], S. KIRAN[a], J. WANG[a], A. H. SHAH[a],
A. ZEGAOUI[a], Y. B. ARSE[a], W. B. LIU[a*]
[a]Key Laboratory of Superlight Material and Surface Technology of Ministry of Education, College of Materials Science and Chemical Engineering, Harbin Engineering University, Harbin, People's Republic of China
[b]Department of Chemical Engineering, Balochistan University of Information Technology, Engineering and Management Sciences, Quetta, Pakistan
[c]Maritime Technologies Complex, Islamabad, Pakistan

The polybenzoxazine and alkali treated waste hemp fibres (HF) composites were prepared by isothermal heating under compression moulding process at 0.05, 0.1, 0.15, 0.2, and 0.3 volume fraction HF loadings. The effects of HF loading on the tensile properties were evaluated and compared with the estimated values of rule of mixture, series, Halpin-Tsai, and Kelly–Tyson models. The series model confirmed that the HFs have a 3D random fibre alignment in the composites. The Kelly–Tyson model was well fitted with the experimental found results for the tensile stress at break, while the Youngs modulus results were best matched with the Halpin-Tsai model predictions. Moreover, the water absorption increased as the HF loadings increased. The Fickian diffusion was observed during the water absorption of the composites. SEM results illustrated that as the HF loading improved the fibre-matrix adhesion was improved.

1. Introduction

The recent studies reflect that the mechanical properties and production techniques of green composites have been extensively focused to fulfil the increasing demand of the public for eco-friendly as well as economical products. The superior specific mechanical properties of bast fibres, such as sisal, flax, kenaf, jute, and hemp fibres (HF), is the major reason for the reinforcement of green materials in composites. The reinforcement of natural fibres (NF) in the polymeric matrix also brings several advantages apart from their low price and biodegradability such as wide availability, on combustion they produce a lower quantity of harmful gases, lower energy requirements, and less wear and tear to machinery during processing. However, the lower compatibility between the hydrophilic nature of NF with hydrophobic matrices is the main disadvantage, they also showed poor environmental stability[1-5].

The reports form Food and Agriculture Organization of United Nation showed the highest HF production in China, last 10 years average production of HF was around 93,000 tons per year. The cellulose (55-78.3%), hemicellulose (10.7-22.4%), lignin (2.9-8.0%), pectin (0.9-18%), and ash (0.8-7.0%) are reported as chemical components of HF[6]. A good portion of HF is discarded as wasted during the separation from hemp bark due to the lower fibre length or diameter. These waste HF can be utilized as a cheap reinforcing material for the polymer composites [7].

Polybenzoxazine polymers showed excellent resistance against the water absorption, moreover, they also have additional advantages such as a near-zero volumetric change on curing, good mechanical and thermal properties[8-10].HF reinforced polybenzoxazine composites have

---

been reported by our group[11, 12]. However, the relationships between the experimental and model expected results are not studied.

In this study, polybenzoxazine reinforced alkali treated HF composites were tested for the tensile and water uptake properties in terms of different HF volume fraction loadings. Moreover, mathematical models were applied to estimate the relationship between the experimental and model results.

2. Materials and methods

2.1. Materials

The Jiangxi Huacui Advanced Materials Co., Ltd. (China) gifted the phenol and 4,4'-diamino diphenylmethane (DDM) based benzoxazine monomer (P-ddm) (99.5%). The waste HF from the bark separation process was friendly provided by Daqing Branch of Heilongjiang Academy of Sciences, Daqing (China). The sodium hydroxide (NaOH) (99.9%), acetic acid (99.0%), cyclohexane (99.5%), and ethanol (99.0%) were procured from Shanghai Jingchun Reagent Co., Ltd., (China).

2.2. Preparation of HF composites

The HFs were subjected to an alkali treatment process with a 5 wt% NaOH solution as stated in our earlier published work [11]. The composites with 0.05, 0.1, 0.15, 0.2, and 0.3 HF volume fraction (V_f) was prepared, V_f was determined by using the following equation [13].

$$V_f = (\rho_f \times \rho_m)/(W_m \times \rho_f + W_f \times \rho_m) \tag{1}$$

where W_m, W_f, ρ_m, and ρ_f represent the weight of the matrix, the weight of fibre, the density of the matrix, and the density of fibre, respectively.

The polybenzoxazine/HF composites were cured by the compression (15 MPa) moulding under isothermal heating at 160, 180, and 200 °C for 2 h each heating stage. The coding and composition of the prepared composites are presented in Table 1.

Table 1. Specimen coding and composition of the HF reinforced polybenzoxazine composites.

Specimen code	P-ddm(Vol. fraction)	Hemp fibre(Vol. fraction)
P(P-ddm)	1	0
P(P-ddm/HF1)	0.05	0.95
P(P-ddm/HF2)	0.90	0.10
P(P-ddm/HF3)	0.15	0.85
P(P-ddm/HF4)	0.80	0.20
P(P-ddm/HF5)	0.70	0.30

2.3. Mathematical models for predictions of tensile properties

The simplest mathematical models for the estimation of composite properties are the rule of mixture (ROM) and the inverse rule of mixture (IROM). The ROM and IROM model are based on two different assumptions; first assumption is that the composites' cumulative property is equal to the sum of all volume fraction of property in materials (ROM model), while the second assumption is both matrix and fibre experienced the same stress (IROM model)[14, 15]. The ROM and IROM models equations are represented as Eq.2 and Eq.3, respectively.

$$P_c = V_m P_m + V_f P_f \tag{2}$$

$$\frac{1}{P_c} = \frac{V_m}{P_m} + \frac{V_f}{P_f} \tag{3}$$

Here P represents the tensile property, such as tensile stress at break (σ) and Young's modulus (E) and V is volume fraction, while subscripted f, m, and c represent fibre, matrix, and composite, respectively.

The ROM model equation was modified for the short fibres reinforced composites, by considering the orientation factor (η_o). The revised ROM equation after considering the η_o is [13]:

$$P_c = V_m P_m + \eta_o V_f P_f$$
$$\tag{4}$$

Several orientation factors (η_o) are available in the literature according to the fibre orientation in the composite, such as $\eta_o=1$ for the uniaxially aligned fibres, $\eta_o=0.375$ for the planar random fibres, and $\eta_o=0.20$ for the three dimensional (3D) random fibres[13].

The semi-empirical equations consider more factors, such as packing arrangement, geometry, and shape factor for fibres, for the prediction of composites properties [15, 16]. The Halpin-Tsai model has been comprehensively applied for the mechanical properties estimation and expressed as:

$$P_c = P_m \left(\frac{1+\varepsilon\eta V_f}{1-\eta V_f}\right) \tag{5}$$

where

$$\eta = \frac{(P_f/P_m)-1}{(P_f/P_m)+\varepsilon}$$

Here ε is known as shape factor and equal to twice of aspect ratio. The Eq. 5 was revised by Tsai for short fibre composites having random fibre orientation. The equation for random-orientated fibres (P_R):

$$P_R = \frac{3}{8}P_L + \frac{5}{8}P_T \tag{6}$$

Here P_L and P_T show the properties share of short fibre composites in longitudinal and transverse directions on same volume fraction, respectively. The value of ε for the P_L and P_T are 2(L/D) and 2, respectively.

The Lewis-Nielsen also modified the Halpin-Tsai model and considered two new factors i.e; the maximum packing of fibre (Φ_m) and dispersion of the fillers (ψ). The Lewis-Nielsen equation is as follows:

$$P_c = P_m \left(\frac{1+\varepsilon\eta V_f}{1-\eta\psi V_f}\right) \tag{7}$$

where

$$\psi = 1 + \left\{\frac{1-\Phi_m}{\Phi_m^2}\right\} V_f$$

Here Φ_m indicates the maximum packing fraction, depends on the arrangement and type of the filler. In our case, short fibres were fillers, while several possibilities of filler arrangement are possible, as uniaxial hexagonal close packing ($\Phi_m= 0.9065$), uniaxial random close packing ($\Phi_m= 0.82$), uniaxial cubic packing ($\Phi_m= 0.785$), and for 3D random packing ($\Phi_m= 0.52$) [17]. A value of 690 MPa and 60 GPa was adopted throughout the estimation of properties for HF as σ and E, respectively [18]. The deviation equation (Eq. 8) was used to estimate the accuracy of the models:

$$\sigma_p = \left[\sum_{i=1}^{n} \frac{\left(P_c^{exp}-P_c^{cal}\right)^2}{n-m}\right]^{1/2} \tag{8}$$

Here P_c^{exp} and P_c^{cal} are the experimental and predicted mechanical properties by using the models, respectively; *n* represents the number of experimental points and *m* presents the adjustable parameter, in the current study *m* was 1.

2.4. Sample characterizations

The digital pictures of HF were recorded by using the optical microscope (Nikon, ECLIPSE E600 POL), and obtained pictures were analyzed by using the *Image J* software for the determination of length and diameter of HF. The tensile tests of $50{\times}10{\times}2$ mm^3 samples were performed on an Instron 5569 instruments, USA, at 1 mm/min crosshead speed to evaluate the tensile properties of HF composites. The ASTM D570–98 standard was followed for estimation of the water uptake behaviour. The water uptake percentage was calculated by using the following formula:

$$W_u = \frac{(W_t - W_o)}{W_o} \times 100 \tag{9}$$

Here W_u represents the water uptake in percentage; while W_t is the weight of the sample at time *t* and W_o represent the weight of the sample before initiating the test. The scanning electron microscope (SEM), CamScan MX 2600FE, Oxford Instruments, UK, at 20 kV accelerating voltage was used to study the morphology of tensile test fracture surfaces. The good repeatability of the data was confirmed by testing at least 5 samples for the same code, and an average value was reported as result.

3. Results and discussion

3.1. Dimensions of reinforced HF

As discussed earlier, the fibre length and diameter always remain a critical factor for the fibre based composites. Fig. 1 presents the distribution of fibre length and fibre aspect ratio (length/diameter) of before and after alkali-treated HF.
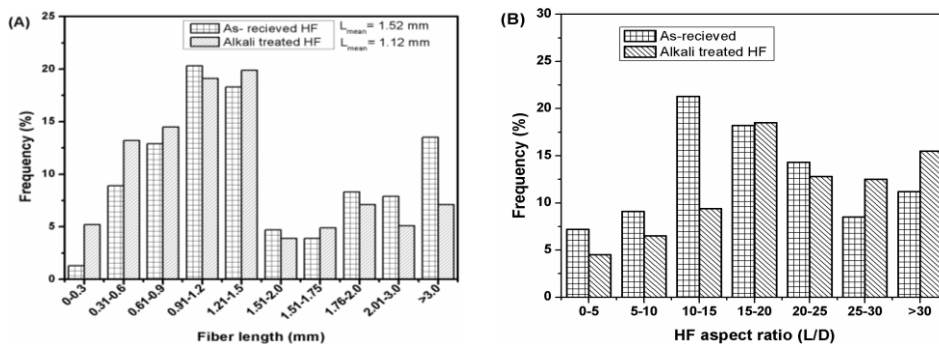

Fig.1. Histogram plot of as-received and alkali treated HF for length (A) and aspect ratio (B).

After the NaOH treatment, microfibrils were observed in the HF; this is an excellent indication of hemicelluloses and lignin removal from the HF surface[19, 20]. Moreover, after the treatment a 27% decline was observed in the average HF length, the average length value reached to 1.12 mm from 1.52 mm. However, the higher impact was observed on the values of average diameter after the NaOH treatment due to observed microfibrils. This noteworthy difference showed the effects by declining the mean aspect ratio value. This is a good sign for the better reinforcement effect of HF in composites.

3.2. Tensile properties

A series of tensile tests were performed to inspect the sound effects of HF loading on σ and E. In addition, the tests results were compared with the estimated values of the analytical models. The tensile test results with standard deviation are summarized in Table 2. The test parameters used for IROM, ROM, modified Halpin-Tsai, and Lewis-Nielsen models and their deviations for tensile test results are presented in Table 3.

Table 2. Tensile test parameters of HF reinforced polybenzoxazine composites.

Sample code	Stress at break(MPa)	Young's modulus (GPa)	Strain(%)
P(P-ddm)	29.02 ± 1.52	1.53 ± 0.165	2.01
P(P-ddm/HF1)	34.46 ± 1.28	2.05 ± 0.109	1.71
P(P-ddm/HF2)	40.21 ± 1.89	2.72 ± 0.187	1.54
P(P-ddm/HF3)	46.32 ± 1.42	3.25 ± 0.179	1.47
P(P-ddm/HF4)	53.26 ± 1.72	3.81 ± 0.215	1.34
P(P-ddm/HF5)	62.93 ± 1.98	5.07 ± 0.239	1.23

Table 3. Test parameters used for IROM, ROM, modified Halpin-Tsai, and Lewis-Nielsen models and their root mean square deviations for tensile test results.

Model	Parameters	σ_σ (MPa)	σ_E(GPa)
IROM	---	15.79	2.07
ROM	η_o=0.20	2.16	0.26
	η_o=0.375	27.22	2.00
	$L/D=10$	32.46	0.45
	$L/D=12$	38.21	0.29
Modified Halpin-Tsai	$L/D=14$	43.24	0.17
	$L/D=16$	47.68	0.12
	$L/D=18$	51.63	0.18
	$\Phi_m = 0.52, L/D=08$	35.87	0.34
Lewis-Nielsen	$\Phi_m = 0.52, L/D=10$	42.41	0.47
	$\Phi_m = 0.52, L/D=12$	48.04	0.72
	$\Phi_m = 0.52, L/D=14$	52.87	1.00

The increase was recorded in the σ and E values as the HF loading increased, and reached at maximum values on 0.3 volume fraction HF loading, which was nearly 112% and 218% higher than the recorded σ and E for native poly(P-ddm), respectively. These remarkable increases in the σ and E values clearly indicate the improved stress transfer. The tensile properties of composites increased, due to the relatively higher tensile properties of neat HF (σ, 690 MPa and E, 60 GPa) and better fibre-matrix adhesion.

The experimental results were compared with the predicted data by using IROM (Eq. 3) and ROM (Eq. 4) models and illustrated as Fig. 2. We can easily observe from Fig. 2, the practical results of σ and E markedly deviate from the IROM model predictions. This recommends that Reuss's assumption is not right for the short fibres reinforced composites. However, it is interesting to observe that the σ and E results were very near to the ROM model prediction on η_o=0.20. This confirms that the dispersion of HF in the composites is in good agreement with the 3D random orientation alignment, especially at a lower loading of HF (0.05, 0.1, and 0.15 volume fraction). As HF loading was increased to 0.2 volume fraction onwards, the σ values moved below than the expected values of ROM at η_o=0.20, while the E values moved away from η_o=0.20 to η_o=0.375. This illustrates that as the fibre loading increased the space for the dispersion of the fibre reduced and amplified the fibre-fibre contact, subsequently the increased fibres dispersed as a 2D random network in a single plane (planar random). Moreover, the lowest deviation values(2.16 MPa and 0.26 GPa) were observed for the ROM model at η_o=0.20 confirmed that the HF were 3D randomly configured in composites.
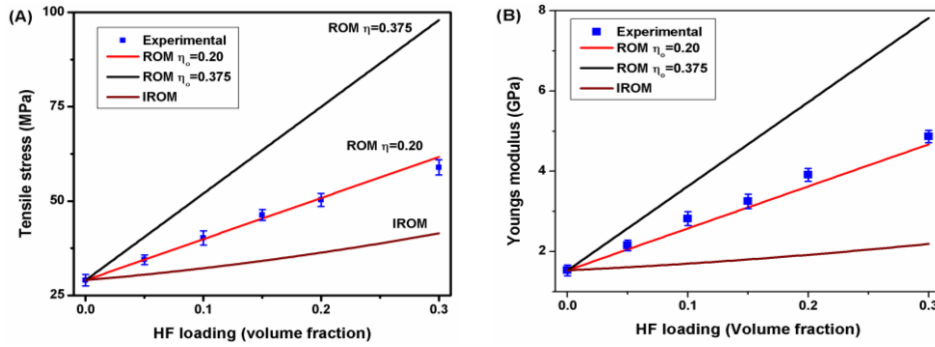
Fig. 2. Experimental and predicted tensile stress at break (A) and Youngs' modulus (B) by using the IROM and ROM models at different orientation factor (η_o).

The predicted results for σ and E at different fibre aspect ratios by using modified Halpin–Tsai (Eq. 6) and Lewis-Nielsen models (Eq. 7) with practically found results are produced as Fig. 3. As it was confirmed by the ROM model that fibre arrangement in the current work was nearby the 3D random fibre orientation line, so a value of 0.52 was used as Φ_m for Lewis-Nielsen model.
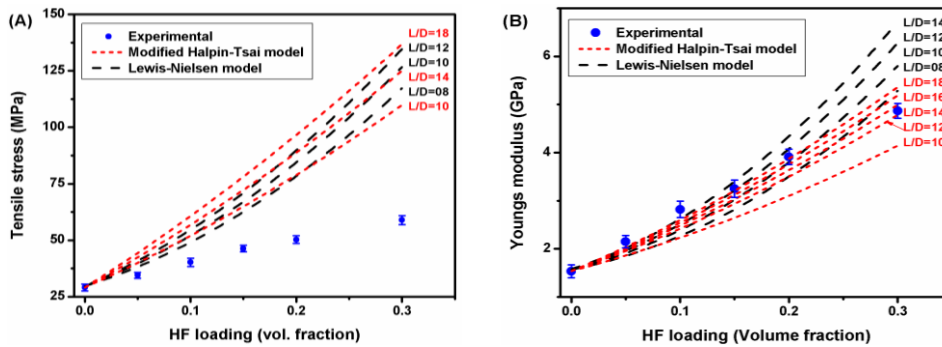

Fig. 3. Tensile stress at break (A) and Youngs' modulus (B) comparison of modified Halpin-Tsai and Lewis-Nielsen model estimations at several HF aspect ratios with the experimental results.

It can be easily observed in Fig. 3A, σ of the composites estimated by using the Halpin–Tsai and Lewis-Nielsen models are significantly lower than the theoretical predictions. The strength value used as σ for the HF was calculated on the long fibre, while short fibre was used in the study. So, it was obvious that both models will overestimate the σ for the composites.

It can be seen from Fig. 3B, the estimated E by using the Lewis-Nielsen model was not accurate to the experimental values especially for P(P-ddm/HF4) and P(P-ddm/HF5) specimen. The high deviations between the model and experimental results suggest that Lewis-Nielsen model is inaccurate for the composites. However, the modified Halpin–Tsai model is in the good agreement with the experimental results, as shown in Fig. 3B. The L/D values before processing were around 22, and considering the decline during mixing and moulding processes, the L/D values of 14-18 for the HF composites was expected. The lowest value of root-mean-square deviations (0.12 GPa) was recorded for the modified Halpin–Tsai model on *L/D=16*. This implies that the Halpin–Tsai model gives better estimations for E than the other models.

3.3. Estimation of σ by Kelly–Tyson model

The Kelly–Tyson model accurately estimates the σ for the short fibre reinforced composites. This model estimates the σ on the concept of constant shear stress applied on the fibres at both ends and results in a linear stress transfer at the fibre–matrix interface. The Kelly–Tyson model is written as [21]:

$$\sigma_c = \left[\eta_o \sum_{l_i<l_c} \frac{\tau l_i V_{f,i}}{2r_f} \right] + \left[\eta_o \sum_{l_j>l_c} \sigma_f V_{f,j}(1 - l_c/2l_j) \right] + \left[\sigma_m(1-V_f) \right] \qquad (9)$$

Here l_i and l_j are the subcritical (i) and supercritical (j) fibre length; l_c is the critical fibre length; $V_{f,i}$ and $V_{f,j}$ are the volume fraction of fibres with l_i and l_j fibre length; r_f is the radius of fibre; and τ is the fibre–matrix interfacial shear stress.

The τ determines the fibre failure mode that either fibre pull-out or breakage was responsible for the failure of the test. The minimum fibre length (l_c) is required to strengthen the composite to their maximum potential, the subcritical fibres having lower lengths than l_c are too short to support the load and cause fibre fracture. Bowyer and Bader stated the relationship of τ with l_c as [21]:

$$l_c = \frac{E_f \varepsilon_c r_f}{\tau} \qquad (10)$$

The stress on composite at break (σ_c) (Eq. 9) can be revised as:

$$\sigma_c = \eta_o (X + Y) + Z \qquad (11)$$

Here X, Y, and Z are contributions from the subcritical length fibres, supercritical length fibres, and matrix, respectively, and can be presented as:

$$X = \left[\eta_o \sum_{l_i<l_c} \frac{\tau l_i V_{f,i}}{2r_f} \right] \qquad (12)$$

$$Y = \left[\eta_o \sum_{l_j>l_c} E_f \varepsilon_c V_{f,i} \left(1 - E_f \varepsilon_c r_f / 2l_j \tau \right) \right] \qquad (13)$$

$$Z = \left[E_m \varepsilon_c (1 - V_f) \right] \qquad (14)$$

First of all, the values E_c at two corresponding volume fraction composite (E_{05} and E_{10}) and their corresponding values for ε (ε_{05} and ε_{10}) and σ (σ_{05} and σ_{10}) were selected and corresponding matrix contributions (Z_{05} and Z_{10}) was estimated by using Eq. 14. Then the deviation value R_z was determined as:

$$R_z = \frac{\sigma_{05} - Z_{05}}{\sigma_{10} - Z_{10}} \qquad (15)$$

Afterwards, a value of τ was assumed and critical fibre length for 0.05 and 0.1 volume fraction HF composite composites (l_{c05} and l_{c10}) was estimated by using the Eq. (10). Then the estimated l_{c05}, l_{c10}, and fibre length distribution data, as described in the earlier section, were used to estimate the contributions from the subcritical and supercritical length fibres by using the Eq.12 and Eq.13. Once again deviation value R_{XY} was determined by the following equation:

$$R_{XY} = \frac{X_{05} + Y_{05}}{X_{10} + Y_{10}} \qquad (16)$$

The values of R_Z and R_{XY} was compared, if there was any difference, the assumed value of τ was adjusted by $\pm$ 0.05 MPa, and the same procedure repeated until the values of R_Z and R_{XY} were same till the third decimal digit. Finally, the value of τ assumed and fibre length distribution data were used to estimate the σ_c by using the Kelly-Tyson model (Eq. 9).

By using the tensile test data and fibre length distribution, the corresponding l_c values were recorded as 1.47, 1.28, 1.16, 1.02, and 0.75 mm, at the 13.9, 14.40, 15.2, 15.70, and 19.45 MPa values of τ for P(P-ddm/HF1), P(P-ddm/HF2), P(P-ddm/HF3), P(P-ddm/HF4), and P(P-ddm/HF5)

composites, respectively. The lower fibre loading samples (P(P-ddm/HF1), P(P-ddm/HF2), and P(P-ddm/HF3) have a larger number shorter HF than their corresponding l_c, as the average HF length was 1.12 mm; so the composites fracture was dominated by fibre pull-out and matrix rapture. From these results, it can be concluded that the lower fibre pull-outs and good fibre-matrix adhesion are expected on higher HF loading (0.2 and 0.3). For P(P-ddm/HF4), and P(P-ddm/HF5) composites, a higher portion of the HF was longer than their l_c, thus, they show much better improvement in the tensile test.

The tensile stress results and the Kelly-Tyson model estimations for the polybenzoxazine reinforced HF composites against different HF volume fraction loadings are presented in Fig.4. The Kelly–Tyson model estimations for the σ_c are a good fit with the practically observed results. Furthermore, on increasing the fibre loading the shifting of fibre alignment from 3D random to planar random was observed, similar behaviour was seen for the ROM model. We can conclude that the predictions made by the Kelly–Tyson model for the tensile strength were much better than the prediction of other semi-empirical models.
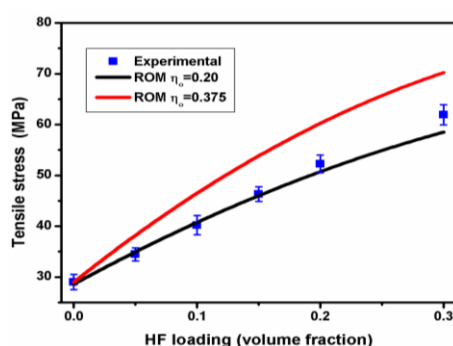

Fig.4. The Kelly–Tyson model estimation at different orientation factor for tensile stress at break and practical found results.

3.4. Water absorption behaviour

The neat polybenzoxazine and HF reinforced polybenzoxazine composites with different volume fraction were studied for water absorption behaviour. The weight gain against the square root of exposure time ($h^{1/2}$) in water for the neat polybenzoxazine and HF composites are illustrated in Fig. 5.

The higher initial water uptake rate and maximum water uptake were observed for all HF composites than the pristine polybenzoxazine resin because HFs are hydrophilic in nature and can absorb more water than the resin. The similar trend was reported by several studies such as hemp [22], jute [23], and sisal [24] reinforced composites. The increase in water uptake is apparent, the reinforcement of HF enhanced the availability of the polar -OH group on the fibre-resin surface [25].

The water adsorption in polymer composites is classified into three categories, namely, Fickian, relaxation-controlled, and non-Fickian or anomalous adsorption. Theoretically, the adsorption type can be easily identified by estimating the rate constants n for the following equation [26].

$$\frac{M_t}{M_{st}} = k\, t^n \tag{17}$$

The experimental data was used to find out the coefficients (n and k). The fitting of the experimental data (intercept and slope) of the $log(M_t/M_{st})$ versus $log(t)$ plot were identified as n and k, respectively. The coefficient of n is used to identify the adsorption type, $n \leq 0.5$ Fickian; relaxation-controlled $n > 0.5$; and anomalous transport $0.5 < n < 1$. The plot of $log(M_t/M_{st})$ versus $log(t)$ and its fitting curves are shown in Fig. 6.

All coefficients of n for the composites were in the range of 0.203 to 0.336 for the water absorption, n values suggest the Fickian diffusion process for the polybenzoxazine /HF

composites. Since the neat polybenzoxazine and its HF composites showed a Fickian like behaviour, the following equation was used to calculate the diffusion constant, D, [19]:

$$\frac{M_t}{M_{st}} = \frac{4}{\sqrt{\pi}}\sqrt{\frac{Dt}{h^2}}$$ (18)

Here M_t and M_{st} are the moisture content at a given time t, and the saturated water uptake, respectively, and h is the thickness of the material. The D was calculated by using the following equation:

$$D = \pi \left[\frac{kh}{4M_{st}}\right]^2$$ (19)

Here k represents the slope which was calculated from the plot of a linear portion of absorbed water against the square root of the time curve.

Table 4 summarizes the absorbed water parameters for polybenzoxazine reinforced HF composites. A rapid increase was seen in the diffusion coefficient values as HF volume fraction increased, the values were recorded to be as 6.66, 7.12, 7.96, 8.27, 8.65, and 10.20 $\times 10^{-9}$ m^2/s for control, 0.05, 0.1, 0.15, 0.2, and 0.3 volume fraction HF composites.
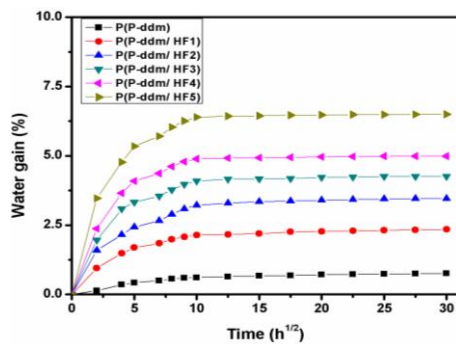

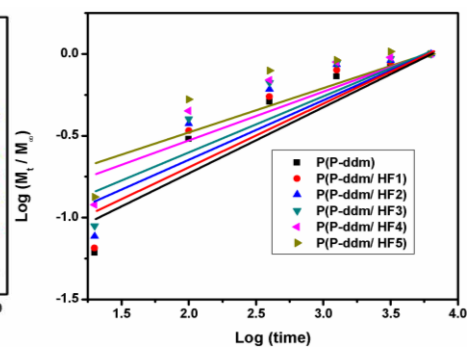Fig. 5. The water absorption curves for the HF reinforced polybenzoxazine composites.

Fig. 6. The log (Mt/Mst) vs. log (t) of the HF reinforced polybenzoxazine composites.

Table 4. Water uptake parameters for HF reinforced polybenzoxazine composites.

Specimen code	M_t versus $t^{1/2}$ plot			log (M_t /M_{st}) versus log (t)	
	Saturated water (M_{st}, %)	Slope of plot (k)	Diffusion coefficient (D, 10^{-9} m^2/s)	n	Slope of plot (k)
P(P-ddm)	0.76	0.056	6.66	0.203	0.451
P(P-ddm/HF1)	2.35	0.179	7.12	0.222	0.440
P(P-ddm/HF2)	3.45	0.278	7.96	0.241	0.414
P(P-ddm/HF3)	4.25	0.349	8.27	0.269	0.391
P(P-ddm/HF4)	4.99	0.419	8.65	0.307	0.343
P(P-ddm/HF5)	6.49	0.481	10.2	0.336	0.323

3.5. Morphology

The tensile test fragment surfaces of HF reinforced composites were studied by using a scanning electron microscope (SEM) for the morphological analysis carried, and presented in Fig. 7. All SEM images clearly show good interfacial wettability due to the absence of voids which reveals the good fibre-matrix adhesion.

It can be easily observed from the morphology of the tensile test fracture surface shown in Fig. 7(A-C)that the fibres were in good adhesion with the matrix, after the tensile stress was applied to the specimen the fibres pull-out from the matrix and then the matrix was broken. After

the increase of HF volume fraction in composite the size of fibre pull-out from the matrix reduced and moved to the fibre breakage in the matrix and improved the tensile properties much linearly (Fig. 7D-E). These SEM images clearly explain the failure morphology of the composites and provide a good explanation for the improved tensile properties.
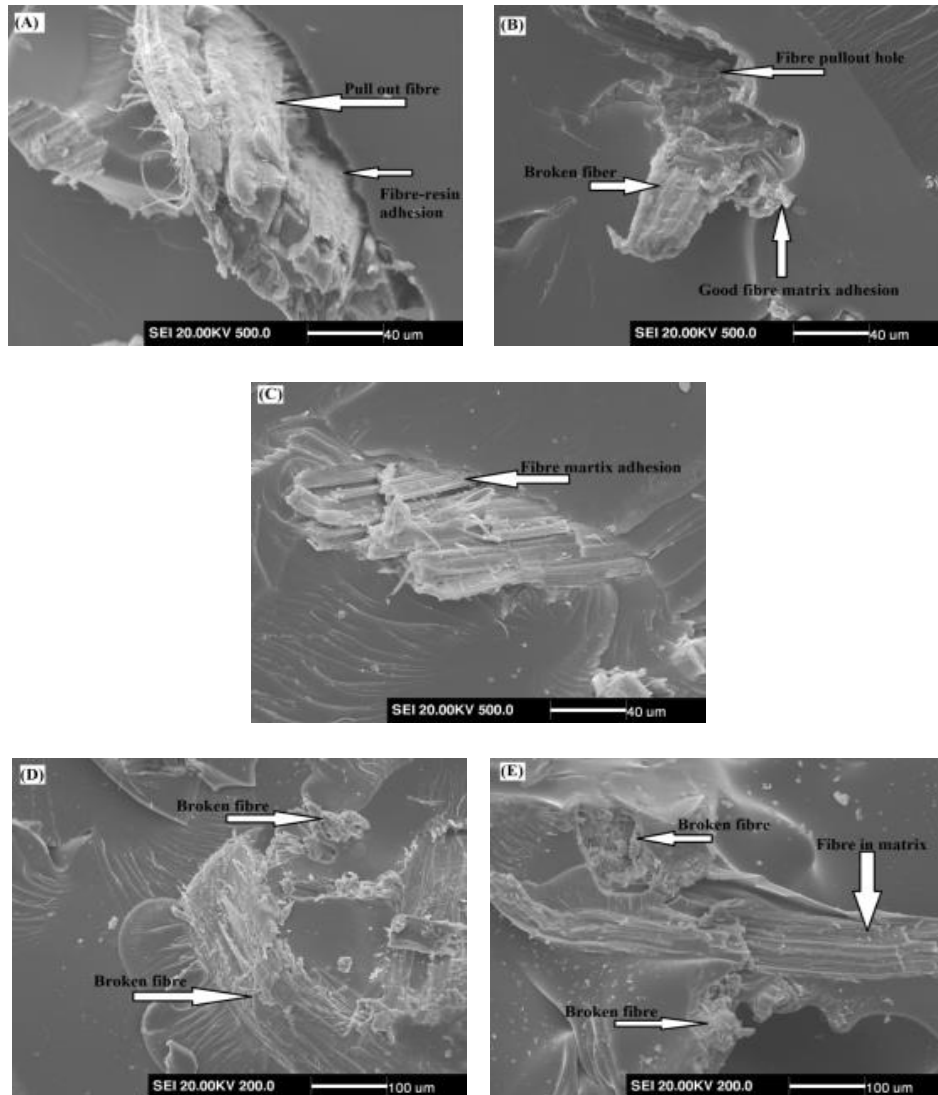

Fig. 7. SEM micrographs of the HF reinforced polybenzoxazine composites at 0.05 (A), 0.1 (B), 0.15 (C), 0.2(D), and 0.3 (E) volume fraction loadings.

4. Conclusion

In the present study, the effects of different HF volume fraction on the tensile and water absorption properties of polybenzoxazine composites were studied and modelled by using the mathematical models. The σ, E, and water absorption were found to increase considerably with HF fibre loading. The ε of the composites was lower than those of neat resins, due to the observed reduction in tensile strain. The σ and E were modelled by using the ROM, series, modified Halpin–Tsai, and Lewis-Nielsen models. The ROM model confirmed that as the fibre loading was increased the fibre alignment was shifting from 3D random to planar random. The Kelly–Tyson model predicted σ more accurately than any other model. The modified Halpin–Tsai model was the best fit for the Youngs modulus on considering the maximum packing fraction. The σ and E were improved by the reinforcement of HF, and increased with the HF loadings; this can be attributed to the good fibre-matrix interactions, as evidenced by the SEM observations. The water

absorption studies on HF composites indicated that Fickian diffusion was observed in all composites. Moreover, higher water was absorbed by the composites on the higher HF loadings.

Acknowledgements

References

[1] A.H. Shah, X. Li, X.D. Xu, S. Wang, J.W. Bai, J. Wang, W.B. Liu, Digest Journal of Nanomaterials and Biostructures **13**, 857(2018).

[2] X. Wu, K. Zhang, Y. Zhang, H. Ji, X. Qu, Digest Journal of Nanomaterials and Biostructures **13**, 399(2018).

[3] A.Q. Dayo, A. Zegaoui, A.A. Nizamani, S. Kiran, J. Wang, M. Derradji, W-a. Cai, W-b. Liu, Materials Chemistry and Physics **217**, 270(2018).

[4] I.D. Ibrahim,T. Jamiru, E.R. Sadiku, W.K. Kupolati, S.C. Agwuncha, G. Ekundayo, Composite Interfaces **23**, 15(2016).

[5] Y-l. Xu, A.Q. Dayo, J. Wang, A-r. Wang, D. Lv, A. Zegaoui, M. Derradji, W-b. Liu, Materials Chemistry and Physics **203**, 293 (2018).

[6] A. Shahzad, Journal of Composite Materials **46**, 973(2012).

[7] B. Lu, L.W. Zhang, J.C. Zeng, Natural fibre composites. Beijing: China Chemical Industry Publishing House (2005).

[8] X. Ning, H. Ishida, Journal of Polymer Science Part A: Polymer Chemistry **32**, 1121(1994).

[9] Y.Yagci, B. Kiskan, N.N. Ghosh, Journal of Polymer Science Part A **47**, 5565 (2009).

[10] N.N. Ghosh, B. Kiskan, Y. Yagci, Progress in Polymer Science **32**, 1344 (2007).

[11] A.Q. Dayo, B-c. Gao, J. Wang, W-b. Liu, M. Derradji, A.H. Shah, A.A. Babar, Composites Science and Technology **144,** 114 (2017).

[12] A.Q.Dayo, Y-l. Xu, A. Zegaoui, A.A. Nizamani, J. Wang, L. Zhang, W-b. Liu, A.H. Shah, Plastics, Rubber and Composites**46,** 442 (2017).

[13] R.F.Gibson, Principle of composite material mechanics, Fourth ed., CRC Press, (2016).

[14] C.L. Tucker, E. Liang, Composites Science and Technology**59,** 655 (1999).

[15] R.M. Jones, Mechanics of composite material, Hemisphere Publishing, USA, (1975).

[16] J.C. Halpin, J.L. Kardos, Polymer Engineering and Science **16**, 344 (1976).

[17] C. Fuchs, D. Bhattacharyya, K. Friedrich, S. Fakirov, Composite Interfaces **13,** 331 (2006).

[18] H.N. Dhakal, Z.Y. Zhang, M.O.W. Richardson, Composites Science and Technology **67**, 1674 (2007).

[19] A.K. Mohanty, A.Wibowo, M. Misra, L.T. Drzal, Composites Part A: Applied Science and Manufacturing **35**, 363 (2004).

[20] M. Das, D. Chakraborty, Journal of Applied Polymer Science **107**, 522 (2008).

[21] W.H. Bowyer, M.G. Bader, Journal of Material Science **7**, 1315 (1972).

[22] A.Q. Dayo, A-r. Wang, S. Kiran, J. Wang, K. Qureshi, Y-l. Xu, A. Zegaoui, M. Derradji, A.A. Babar, W-b. Liu, Industrial Crops and Products **111**, 277 (2018).

[23] J. Gassan, A.K. Bledzki, Polymer Composites **18**, 179 (1997).

[24] T.P. Mohan, K. Kanny, Composites Part A: Applied Science and Manufacturing **42**, 385 (2011).

[25] M.N. Ichazo, C.Albano, J. González, R. Perera, M.V. Candal, Composite Structures **54**, 207 (2001).

[26] P. Neogi, Diffusion in Polymers, Marcel Dekker: New York, (1996).